Article Beitr. Phys. Atmosph., May 1994, p. 97–102
0005-8173/94/02 0097–06 $ 3.00/0 Vol. 67, No. 2 97

Frictional Effects on Cold Fronts: Geometric Considerations

by D. HEIMANN

Institut für Physik der Atmosphäre, Deutsche Forschungsanstalt für Luft- und Raumfahrt (DLR), Oberpfaffenhofen, 82234 Weßling, Germany

(Manuscript received August 15, 1993; accepted March 21, 1994)

Abstract

The effect of frictionally induced wind shift and speed reduction on the cross-front wind component is studied for a moving system of two homogeneous air masses. With the aid of a simple geometric conception it is shown that friction tends to intensify the cross-front wind component at the rear side of the front and thus accelerates the frontal progress unless the temperature jump at the frontal surface is small or the angle between the geostrophic flow in the warm air and the surface front line is very acute. The findings from the geometric consideration turned out to be in qualitative agreement with the results of two-dimensional numerical simulations.

Zusammenfassung

Reibungseffekte an Kaltfronten: geometrische Betrachtungen

Der Effekt der reibungsbedingten Winddrehung und Geschwindigkeitsreduktion auf die frontnormale Windkomponente wird für ein bewegtes, aus zwei homogenen Luftmassen bestehendes System betrachtet. Anhand eines einfachen geometrischen Konzepts wird gezeigt, daß die front-normale Windkomponente auf der Rückseite der Front im Vergleich zur geostrophischen Komponente durch die Reibung verstärkt wird, es sei denn, daß der Temperatursprung an der Frontfläche klein oder der Winkel zwischen dem geostrophischen Wind in der Warmluft und der Bodenfrontlinie sehr spitz ist. Die Erkenntnisse der geometrischen Betrachtungen erwiesen sich in qualitativer Übereinstimmung mit den Ergebnissen zweidimensionaler numerischer Simulationen.

1 The Problem

The cross-isobaric flow component in the Ekman-layer leads to convergent flow in regimes of cyclonic geostrophic vorticity, i.e. Ekman-pumping. Since the pressure field at moving cold fronts shows almost a first order discontinuity at fronts with a cyclonic kink of the isobars, the convergence is well pronounced immediately at the front line. It is therefore expected that frictional effects contribute significantly to the low-level vertical circulation at surface fronts.

Ekman boundary-layer considerations would also suggest that, depending upon the direction of the postfrontal geostrophic flow, the frictionally induced wind shift and speed reduction may either weaken or intensify the postfrontal cross-front wind component. Hence, it is also expected that the speed of the front might be modified by frictional effects. This was addressed, for instance, by Heimann (1992) in the discussion of numerically simulated fronts that were found to travel at different speed if the cross-front temperature contrast or the large-scale pressure field were altered.

Egger (1988) investigated the frictionally induced circulation in a stationary front of the Margules type. In this spacial case the isobars are parallel to the front so that the cross-front component of the geostrophic wind is zero.

In the following an estimate is derived for the above mentioned frictional effects under large-scale conditions that are similar to those of the numerical experiments of Heimann (1992). In effect there are sufficient degrees of freedom for the front to move and for the pressure to vary along the front.

2 Conceptual Model

We consider a simple system of two air masses with constant potential temperatures θ_1 and θ_2 ($\theta_1 > \theta_2$), which are separated by an inclined frontal surface at a height $H_F(x)$. We choose the coordinate system such that the x-axis is perpendicular to the surface front with the surface front at x = 0. At a given time t_0 the flow is defined to be in geostrophic balance except for the surface-based layer below H_E, i.e. the boundary layer, where a geostrophic-antitriptic equilibrium is assumed. The air below H_E is considered to be vertically well mixed such that the air-mass boundary, i.e. the frontal surface, is upright (see upper part of Figure 1).

Hence, the system at time t_0 is described by

$$-f(v_{gi} - v_i) - R_{ui} = 0 \tag{1a}$$

$$+f(u_{gi} - u_i) - R_{vi} = 0 \tag{1b}$$

with $R_{ui} = R_{vi} = 0$ for $z \geq H_E$ and i denoting warm air (i = 1) and cold air (i = 2), respectively. Above H_E the equations (1a, 1b) reduce to $u_i = u_{gi}$ and $v_i = v_{gi}$, where u_{gi}, v_{gi} are the respective geostrophic wind components.

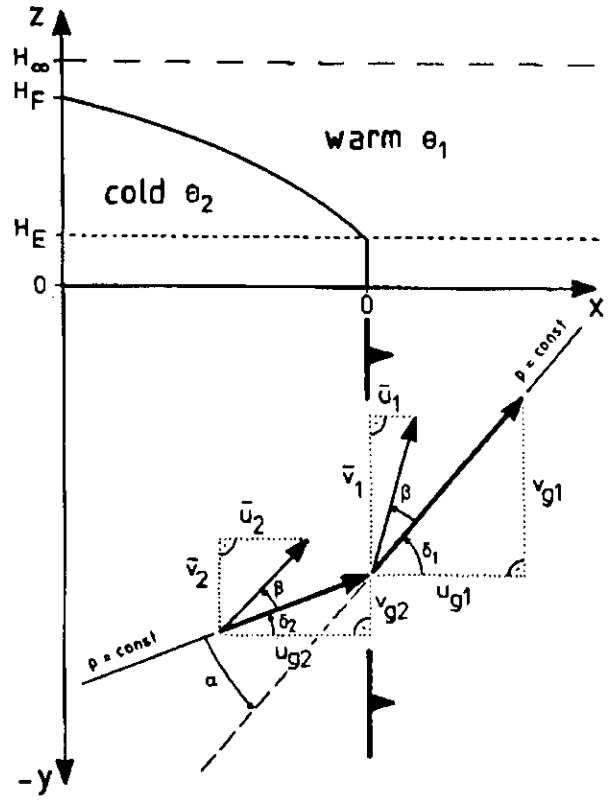

Figure 1 Schematic representation of the cold front in the vertical x–z-plane (upper part) and definition of wind components and angles in a horizontal x–y-plane below H_E (lower part).

For H_F we adapt the solution obtained by Davies (1984) for a steadily moving cold front with constant potential vorticity $PV = f/H_{F\infty}$ in the cold-air layer:

$$H_F(x) = \Delta H_{F\infty}\left(1 - \exp\left(\frac{f}{(g'\Delta H_{F\infty})^{1/2}}\, x\right)\right) + H_E$$

$$\text{for } x \leq 0 \tag{2}$$

with $g' = g\Delta\theta/\theta_2$, $\Delta\theta = \theta_1 - \theta_2$ and $\Delta H_{F\infty} = H_{F\infty} - H_E$.

$H_{F\infty}$ is the maximum thickness of the cold air layer that is reached asymptotically for $x \to -\infty$. A vertical section through this system is presented in the upper part of Figure 1.

The geostrophic wind components in the warm air (u_{g1} and v_{g1}) are prescribed. The geostrophic wind components in the post-frontal cold air, i.e. beneath H_F, are then given by $u_{g2} = \varepsilon u_{g1}$ and $v_{g2} = \varepsilon v_{g1} + g'/f\partial H_F/\partial x$ with $\varepsilon = \theta_2/\theta_1 < 1$.

Smith (1990) points to the fact that $u_{g1} > u_{g2}$ implies an infinite divergence at the frontal surface, which, in turn, has the consequence that the warm air, which overlies the cold air (for $x < 0$), must subside. In our considerations we simplify the problem and substitute θ_1 and θ_2 by a mean potential temperature in the determination of ε so that ε becomes unity. In the calculation of g', however, θ_1 and θ_2 remain unchanged. This accords with the common Boussinesq approximation where a mean density is used in the horizontal pressure terms and deviations from that mean are considered in the buoyancy term only. We put up with the dynamic inconsistency of this approximation since the implied inaccuracy of geostrophic wind components is small compared with the frictionally induced deviation from geostrophy. With $\varepsilon = 1$ the expressions for u_g and v_g reduce to

$$u_g = u_{g1} = u_{g2} \tag{3}$$

and

$$v_{g2} = v_{g1} + \frac{g'}{f}\frac{\partial H_F}{\partial x} \tag{4}$$

In the frictionless case the speed of the front c_F is determined by the speed of the cross-front wind component in the cold air u_2, which then equals the cross-front geostrophic wind component u_g. In this case the above defined system keeps its geostrophic balance and moves with a steady speed $c_F = u_g$ for all times $t > t_0$.

Frictional effects on the movement of the front are assessed by the bulk cross-front wind components $\bar{u}_1$ and $\bar{u}_2$ in the boundary layer on both sides of the

front. From Figure 1 it is obvious that $\bar{u}_1$ and $\bar{u}_2$ are given by

$$\bar{u}_i = R\,(u_g \cos\beta - v_{gi} \sin\beta) \quad i = 1,2 \tag{5}$$

where R and β represent the fraction by which friction reduces the speed and the angle by which friction turns the wind out of the geostrophic direction, respectively. In order to obtain appropriate values for R and β we assume that the bulk boundary-layer wind components correspond with the vertically averaged Ekman solution. The vertical integration of the Ekman equation over the full extent of the Ekman layer $0 \le z \le H_E$ leads to expressions that are independent of the Ekman-layer thickness H_E itself:

$$R = \left[1 - \frac{1+\exp(-\pi)}{\pi} + \frac{1+\exp(-\pi)^2}{2\pi^2}\right]^{0.5} = 0.848$$

$$\beta = \tan^{-1}\left[1 - \frac{1-\exp(-\pi)}{2\pi - \exp(-\pi) - 1}\right] = 10.35°$$

Since u_g and v_{g1} are prescribed, the solution of (5) still requires an expression for v_{g2}.

From simple trigonometry (see x – y – plane in Figure 1) follows that

$$v_{g1} = u_g \tan\delta_1 \tag{6}$$

and

$$v_{g2} = u_g \tan\delta_2 \tag{7}$$

where $\alpha = \delta_1 - \delta_2$ is the angle by which the isobars are bent at the front.

With Eq. (7) and trigonometric manipulations we obtain the following expression for the angle α:

$$\alpha = \tan^{-1}\frac{\tan\delta_1 - \frac{v_{g2}}{u_g}}{1 + \frac{v_{g2}}{u_g}\tan\delta_1} \tag{8}$$

where the geostrophic component v_{g2} will be eliminated by

$$v_{g2} = u_g \tan\delta_1 + \frac{g'}{f}\frac{\partial H_F}{\partial x} \tag{9}$$

which follows from Eq. (4) and (6).

The spatial derivation of (2) at the surface front position x = 0 yields

$$\frac{\partial H_F}{\partial x} = -\frac{f}{g'}\,(g'\Delta H_{F\infty})^{1/2} \tag{10}$$

After substituting (10) in (9) the along-front component of the geostrophic wind on the cold-air side of the surface front is expressed by

$$v_{g2} = u_g \tan\delta_1 - (g'\Delta H_{F\infty})^{1/2} \tag{11}$$

Finally, we substitute the geostrophic components in Eq. (5) by (6) and (11) and arrive with the following equations for the vertically averaged Ekman-layer cross-front wind components on both sides of the surface front:

$$\bar{u}_1 = R\,[u_g(\cos\beta - \tan\delta_1 \sin\beta)] \tag{12}$$

$$\bar{u}_2 = R\,[u_g(\cos\beta - \tan\delta_1 \sin\beta)] + R \sin\beta\,(g'\Delta H_{F\infty})^{1/2} \tag{13}$$

3 Results

In the following we choose $u_g = 10$ m/s and $\Delta H_{F\infty} = 9000$ m as a standard parameter setting. The behaviour of α, δ_2 and $\bar{u}_2/u_g$ is visualized in Figures 2 and 3 in the range $0 < \Delta\theta \le 10$ K and $0 \le \delta_1 < 90°$.

Figures 2 shows the variation of the angles α and δ_2. They represent the bend of the isobars at the front and the direction of the post-frontal geostrophic flow, respectively. The angle α is greatest for δ_1 near 60°. It is obtuse only for small values of $\Delta\theta$ or for fronts which are preceded by an almost frontal-parallel warm-air flow. The angle δ_2 is negative for a wide range of $\Delta\theta$ and δ_1. This implies that, in general, the post-frontal geostrophic flow has a northerly component, provided the x-axis points to the east. For large values of δ_1 (almost front-parallel geostrophic flow in the warm air) or small values of

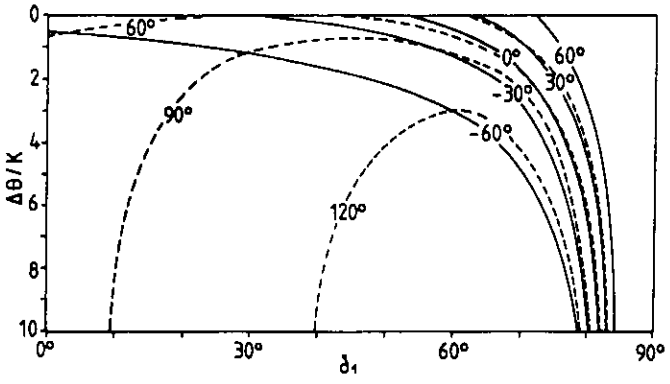

Figure 2 Variation of δ_2 (solid isolines) and α (broken isolines) displayed as a function of δ_1 and $\Delta\theta$ for $u_g = 10$ m/s and $H_{F\infty} = 9000$ m.

$\Delta\theta$, however, the post-frontal geostrophic flow shows a southerly component.

The friction causes the boundary-layer wind to turn in counter-clockwise direction (in the northern hemisphere). Depending on the direction of the geostrophic flow the boundary-layer wind turns towards the front or away from it, thereby increasing or decreasing its component perpendicular to the front. Disregarding the frictional reduction of speed, the frictional wind shift tends to increase the cross-front wind component only if $\delta_1 < -\beta/2$ in the warm air and $\delta_2 < -\beta/2$ in the cold air. On the other hand, the cross-front component even reverses its sign for $\delta_i < -\pi/2 - \beta$ $(i = 1,2)$. In the warm air friction always tends to reduce the cross-front wind component relative to the geostrophic value and may even lead to a boundary-layer flow towards the front for large values of δ_1, i.e. for a nearly front-parallel geostrophic flow.

Since friction also causes a reduction of speed, the situation becomes a little more complex. The combined effect of speed reduction and wind shift is illustrated in Figure 3, where the ratio $\bar{u}_2/u_g$ is plotted as a function of $\Delta\theta$ and δ_1. On the cold side of the front friction intensifies the cross-front component $\bar{u}_2$ for a wide range of $\Delta\theta$ and δ_1. Only if the warm-air geostrophic wind vector does not deviate much from the orientation of the front line or $\Delta\theta$ is rather small, friction tends to weaken $\bar{u}_2$. If the geostrophic flow in the warm air is almost parallel to the front the cross-front component even reverses its sign so that the post-frontal wind is directed away from the front.

The effect of alternative sets of u_g, and $H_{F\infty}$ on the isoline $\bar{u}_2/u_g = 1$ is depicted in Figure 4. It shows that a frictional induced intensification of the cross-front component appears for a wider range of u_g and $\Delta\theta$ if the cross-front geostrophic component u_g is halved. If, on the other hand, the maximum height of the cold-air layer $H_{F\infty}$ is halved, the frictional induced intensification of u_2 is restricted to situations with small values of δ_1 and high values of $\Delta\theta$. It is even more restricted, if u_g is doubled.

4 Relevance of the Geometric Consideration

We consider a situation as defined in Figure 1 to be valid at a certain time $t = t_0$. A short time later, say at $t = t_0 + \delta t$, the cross-front geostrophic wind component has moved the front by $\delta x = u_g \cdot \delta t$. Within the Ekman layer, however the front is moved by $\bar{u}_2$ rather than by u_g. Depending on

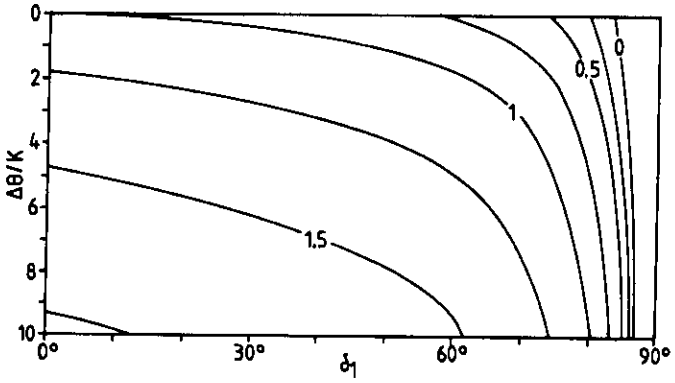

Figure 3 The ratio $\bar{u}_2/u_g$ displayed as a function of δ_1 and $\Delta\theta$ for $u_g = 10$ m/s and $H_{F\infty} = 9000$ m.

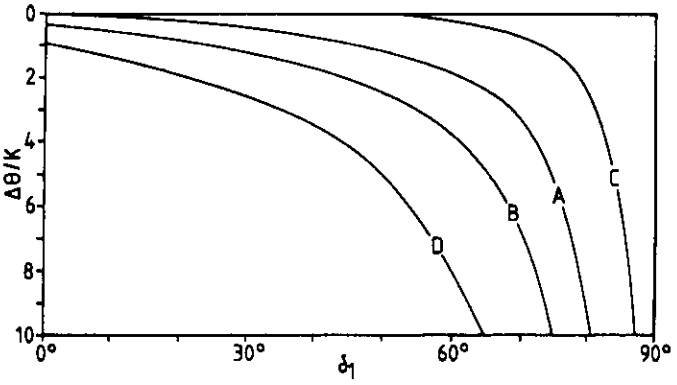

Figure 4 Isolines of $\bar{u}_2/u_g = 1$ for different parameter settings. A: for the standard parameter setting ($u_g = 10$ m/s, $H_{F\infty} = 9000$ m). B: as for A but with $H_{F\infty} = 4500$ m. C: as for A but with $u_g = 5$ m/s, D: as for A but with $u_g = 20$ m/s. The ratio $\bar{u}_2/u_g$ exceeds unity below the respective isolines.

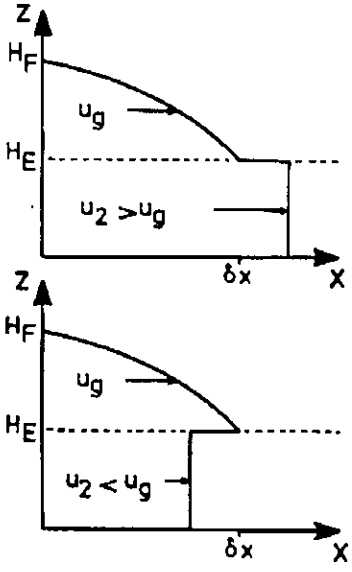

Figure 5 Schematic view of the frontal surface after a small time step $\delta t = \delta x/\bar{u}_2$ for $\bar{u}_2/u_g > 1$ (top) and $\bar{u}_2/u_g < 1$ (bottom).

whether $\bar{u}_2$ exceeds u_g or not the boundary-layer front precedes the upper-air front or lags behind. Both situations are schematically depicted in Figure 5. It is obvious that the assumptions of the geometric considerations, in particular the validity of Eq. (6) and (11), are now no longer fulfilled. In the case $\bar{u}_2 > u_g$ the frontal surface formes a plateau before it ascends according to Eq. (2). This modification changes the cross-front pressure gradient and therewith the along-front component of the geostrophic wind immediately behind the surface front. The along-front component of the geostrophic wind is accordingly changed in the case $\bar{u}_2 < u_g$, but this time immediately ahead of the surface front. Moreover, the cold air superimposes the warm air in front of the surface front in that case. This implies an unstable stratification, which, in turn, causes enhanced turbulent mixing. Hence, it is expected that the speed of the surface front c_F deviates more or less from the values of $\bar{u}_2$ as obtained from Eq. (13).

In order to prove the relevance of the geometric consideration for the estimation of the frontal propagation speed two-dimensional numerical simulations were performed under more realistic conditions. The applied model is a two-dimensional version of the three-dimensional hydrostatic model that was already used for numerical experiments dealing with the interaction of fronts and orography (Heimann, 1990, 1992). The initial conditions of the model runs were chosen such that they conform to the situation sketched in Figure 2. Different from the simple geometric consideration the vertical resolution of the model (20 layers in the troposphere, nine of them employed below 3 km) allows for realistic wind profiles in the boundary layer. The friction is introduced by a prognostic equation for the turbulent kinetic energy E which considers the production of turbulence by both vertical wind shear and buoyancy. The diffusion coefficient K is derived using the relation

$$K = \ell \frac{u_* \sqrt{0.2\,E}}{k\,z\,\partial u/\partial z}$$

with ℓ, u_*, and k being the mixing length, the friction velocity, and the Karman constant, respectively. The lateral boundary condition guarantees the inflow of cold air with a thickness that increases in conformity with Eq. (2).

Nine simulations were performed for combinations of $\delta_1 = 50°$, 60°, 70° and $\Delta\theta = 3$ K, 6 K, 9 K. For the other parameters the standard set was used, i.e. $H_{F\infty} = 9000$ m and $u_g = 10$ m/s. Figure 6 illustrates the results of the simulations for $\Delta\theta = 6$ K, $\delta_1 = 50°$ and $\delta_1 = 70°$ in comparison with the purely geostrophic, i.e. frictionless, movement. The graphic shows a vertical section of the leading edge of the frontal layer after 6 and 12 hours of temporal integration. The influence of friction is evident. Compared with the geostrophic translation the speed of the surface front is retarded in the case with the higher value of δ_1 while it is increased in the other case. The shape of the frontal surface resembles the schematic representation (Figure 5) in either case. For $\delta_1 = 50°$ the frontal surface is almost upright near the ground, but then forms a plateau before it continuously extends to higher altitudes. For $\delta_1 = 70°$ the frontal surface is even tilted backward near the ground indicating static instability.

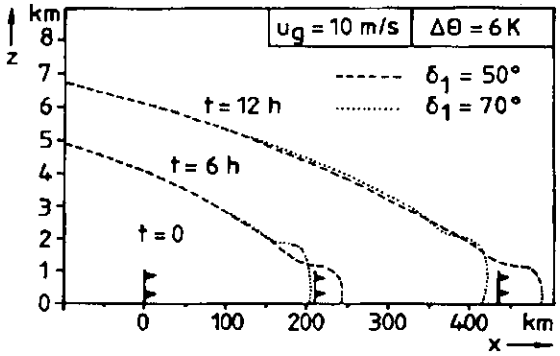

Figure 6 Vertical section showing the leading frontal surface as simulated by the two-dimensional numerical model after 6 and 12 hours. The cases with friction are plotted with dashed ($\delta_1 = 50°$) and dotted ($\delta_1 = 70°$) lines. The cold front symbols indicate the respective positions of a geostrophically translated (no friction) front.

Table 1 The speed ratio c_F/u_g simulated by the two-dimensional numerical model as a function of the cross-frontal temperature difference ($\Delta\theta$) and the deviation of the prefrontal geostrophic flow direction from the front-normal direction (δ_1). The corresponding solutions of Eq. (13) $\bar{u}_2/u_g$ are set in parentheses for comparison.

	δ_1		
$\Delta\theta$	50°	60°	70°
3 K	1.030 (1.121)	0.972 (1.039)	0.845 (0.884)
6 K	1.134 (1.315)	1.076 (1.233)	0.972 (1.078)
9 K	1.192 (1.464)	1.146 (1.381)	1.041 (1.228)

The results of all numerical simulations are given in Table 1. The values represent the average frontal speeds c_F in the period $0 \leq t \leq 12$ h. In this period the fronts move almost steadily with different speeds. For longer periods, however, the speeds tend to assimilate.

The table compares the simulated speed ratios c_F/u_g with the corresponding ratios $\bar{u}_2/u_g$ as obtained from Eq. (13) (in parantheses). The qualitative agreement of the dependency on δ_1 and $\Delta\theta$ is striking. The simulated ratios, however, are much closer to unity than those calculated by Eq. (13). This means that dynamic and frictional forces, which belong to the modified along-front component of the geostrophic wind and the enhanced turbulence, respectively, couple the surface front with the cross-front geostrophic flow.

5 Conclusion

Simple geometric considerations of an idealized cold front yielded an analytic solution for the cross-front wind component in the Ekman-layer on the rear side of the front. This wind component, which transports the properties of the post-frontal cold air, was found to exceed the prescribed cross-front geostrophic wind component for a great range of the temperature difference between the involved air masses and the angle between the prefrontal geostrophic wind direction and the front-normal direction, except for small temperature differences or large angles.

The applicability of the geometric approach is, of course, limited. First, the use of balanced air mass model for moving fronts is questionable as Smith (1992) pointed out. Second, the assumption on which the Ekman solution is based, is not, if at all, fulfilled near fronts where the air is normally out of geostrophic-antitriptic equilibrium. Additional caution is necessary in estimating the speed of a front simply from the increase or decrease of the cross-front wind component due to friction. Nevertheless, the results of the geometric consideration are in qualitative agreement with two-dimensional model simulations. They corroborate the assumption that, for a given cross-front component of the geostrophic wind, the frictionally influenced speed of a cold front depends on the warm-air geostrophic wind direction and the cross-front temperature contrast.

References

Davies, H. C., 1984: On the orographic retardation of a cold front. Beitr. Phys. Atmosph. **57**, 409–418.

Egger, J., 1988: Frictionally induced circulations in fronts. Beitr. Phys. Atmosph. **61**, 140–142.

Heimann, D., 1990: Three-dimensional modelling of synthetic cold fronts approaching the Alps. Meteorol. Atmos. Phys. **42**, 197–219.

Heimann, D., 1992: Three-dimensional modelling of synthetic cold fronts interacting with northern Alpine foehn. Meteorol. Atmos. Phys. **48**, 139–163.

Smith, R. K., 1990: Translation of balanced air mass models of fronts and associated surface pressure changes. Mon. Wea. Rev. **118**, 1922–1926.

front. From Figure 1 it is obvious that $\bar{u}_1$ and $\bar{u}_2$ are given by

$$\bar{u}_i = R\,(u_g \cos\beta - v_{gi} \sin\beta) \quad i = 1,2 \tag{5}$$

where R and β represent the fraction by which friction reduces the speed and the angle by which friction turns the wind out of the geostrophic direction, respectively. In order to obtain appropriate values for R and β we assume that the bulk boundary-layer wind components correspond with the vertically averaged Ekman solution. The vertical integration of the Ekman equation over the full extent of the Ekman layer $0 \le z \le H_E$ leads to expressions that are independent of the Ekman-layer thickness H_E itself:

$$R = \left[1 - \frac{1+\exp(-\pi)}{\pi} + \frac{1+\exp(-\pi)^2}{2\pi^2}\right]^{0.5} = 0.848$$

$$\beta = \tan^{-1}\left[1 - \frac{1-\exp(-\pi)}{2\pi - \exp(-\pi) - 1}\right] = 10.35°$$

Since u_g and v_{g1} are prescribed, the solution of (5) still requires an expression for v_{g2}.

From simple trigonometry (see x – y – plane in Figure 1) follows that

$$v_{g1} = u_g \tan\delta_1 \tag{6}$$

and

$$v_{g2} = u_g \tan\delta_2 \tag{7}$$

where $\alpha = \delta_1 - \delta_2$ is the angle by which the isobars are bent at the front.

With Eq. (7) and trigonometric manipulations we obtain the following expression for the angle α:

$$\alpha = \tan^{-1}\frac{\tan\delta_1 - \frac{v_{g2}}{u_g}}{1 + \frac{v_{g2}}{u_g}\tan\delta_1} \tag{8}$$

where the geostrophic component v_{g2} will be eliminated by

$$v_{g2} = u_g \tan\delta_1 + \frac{g'}{f}\frac{\partial H_F}{\partial x} \tag{9}$$

which follows from Eq. (4) and (6).

The spatial derivation of (2) at the surface front position x = 0 yields

$$\frac{\partial H_F}{\partial x} = -\frac{f}{g'}\,(g'\Delta H_{F\infty})^{1/2} \tag{10}$$

After substituting (10) in (9) the along-front component of the geostrophic wind on the cold-air side of the surface front is expressed by

$$v_{g2} = u_g \tan\delta_1 - (g'\Delta H_{F\infty})^{1/2} \tag{11}$$

Finally, we substitute the geostrophic components in Eq. (5) by (6) and (11) and arrive with the following equations for the vertically averaged Ekman-layer cross-front wind components on both sides of the surface front:

$$\bar{u}_1 = R\,[u_g(\cos\beta - \tan\delta_1 \sin\beta)] \tag{12}$$

$$\bar{u}_2 = R\,[u_g(\cos\beta - \tan\delta_1 \sin\beta)] + R \sin\beta\,(g'\Delta H_{F\infty})^{1/2} \tag{13}$$

3 Results

In the following we choose $u_g = 10$ m/s and $\Delta H_{F\infty} = 9000$ m as a standard parameter setting. The behaviour of α, δ_2 and $\bar{u}_2/u_g$ is visualized in Figures 2 and 3 in the range $0 < \Delta\theta \le 10$ K and $0 \le \delta_1 < 90°$.

Figures 2 shows the variation of the angles α and δ_2. They represent the bend of the isobars at the front and the direction of the post-frontal geostrophic flow, respectively. The angle α is greatest for δ_1 near 60°. It is obtuse only for small values of $\Delta\theta$ or for fronts which are preceded by an almost frontal-parallel warm-air flow. The angle δ_2 is negative for a wide range of $\Delta\theta$ and δ_1. This implies that, in general, the post-frontal geostrophic flow has a northerly component, provided the x-axis points to the east. For large values of δ_1 (almost front-parallel geostrophic flow in the warm air) or small values of

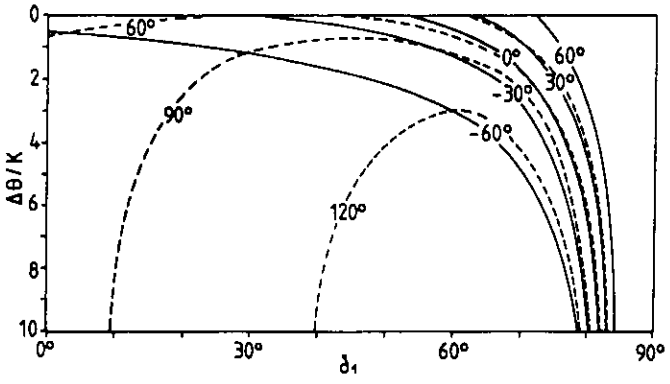

Figure 2 Variation of δ_2 (solid isolines) and α (broken isolines) displayed as a function of δ_1 and $\Delta\theta$ for $u_g = 10$ m/s and $H_{F\infty} = 9000$ m.